

PLANET HUNTERS X: SEARCHING FOR NEARBY NEIGHBORS OF 75 PLANET AND ECLIPSING BINARY CANDIDATES FROM THE K2 *KEPLER* EXTENDED MISSION

JOSEPH R. SCHMITT¹, ANDREI TOKOVININ², JI WANG³, DEBRA A. FISCHER¹, MARTTI H. KRISTIANSEN^{4,5},
 DARYLL M. LACOURSE⁵, ROBERT GAGLIANO⁵, ARVIN JOSEFF V. TAN⁵, HANS MARTIN SCHWENGELER⁵, MARK R.
 OMOHUNDRO⁵, ALEXANDER VENNER⁵, IVAN TERENTEV⁵, ALLAN R. SCHMITT⁵, THOMAS L. JACOBS⁵, TROY
 WINARSKI⁵, JOHANN SEJPKA⁵, KIAN J. JEK⁵, TABETHA S. BOYAJIAN¹, JOHN M. BREWER¹, SASCHA T.
 ISHIKAWA⁶, CHRIS LINTOTT⁷, STUART LYNN^{6,8}, KEVIN SCHAWINSKI⁹, AND ALEX WEIKSNAR⁶

(Accepted in AJ on March 15, 2016)

ABSTRACT

We present high resolution observations of a sample of 75 K2 targets from Campaigns 1-3 using speckle interferometry on the Southern Astrophysical Research (SOAR) telescope and adaptive optics (AO) imaging at the Keck II telescope. The median SOAR *I*-band and Keck *K_s*-band detection limits at 1'' were $\Delta m_I = 4.4$ mag and $\Delta m_{K_s} = 6.1$ mag, respectively. This sample includes 37 stars likely to host planets, 32 targets likely to be EBs, and 6 other targets previously labeled as likely planetary false positives. We find nine likely physically bound companion stars within 3'' of three candidate transiting exoplanet host stars and six likely eclipsing binaries (EB). Six of the nine detected companions are new discoveries, one of them associated with a planet candidate (EPIC 206061524). Among the EB candidates, companions were only found near the shortest period ones ($P < 3$ days), which is in line with previous results showing high multiplicity near short-period binary stars. This high resolution data, including both the detected companions and the limits on potential unseen companions, will be useful in future planet vetting and stellar multiplicity rate studies for planets and binaries.

Subject headings: planetary systems — binaries: general — binaries: eclipsing — techniques: high angular resolution

1. INTRODUCTION

The multiplicity of stellar systems has been well studied (Duchêne & Kraus 2013), from M-dwarfs (e.g., Fischer & Marcy 1992; Dieterich et al. 2012) to solar-type stars (e.g., Abt & Levy 1976; Tokovinin 2014) to higher mass stars (e.g., Garmany et al. 1980; Sana et al. 2012). High resolution imaging is an effective method for searching for companion stars. Adaptive optics (AO) is one such method, which uses natural or laser guiding stars to measure the air turbulence and deformable mirrors to correct for it, improving the angular resolution of astronomical images. AO usually provides the highest resolution for ground-based methods outside of long baseline interferometry. Speckle

methods, on the other hand, take many images of the target star with millisecond exposures (a data cube), essentially freezing the air turbulence in place for the duration of the short observation, allowing for diffraction-limited resolution, as opposed to seeing-limited. With speckle interferometry, a Fourier analysis of every frame is performed to find nearby companions (e.g., Howell et al. 2011). With lucky imaging, a subset of only the best frames are selected for analysis (e.g., Daemgen et al. 2009). In this paper, we perform AO and speckle observations to search for companion stars to planet host stars or eclipsing binary (EB) candidates from the extended *Kepler* mission (K2).

2. TARGET SELECTION

The *Kepler* mission (Borucki et al. 2010) observed $\sim 160,000$ stars almost continuously for nearly four years searching for planetary transits. The mission discovered more than 1000 planets and another ~ 3700 planet candidates¹⁰ (Coughlin et al. 2015). In May, 2013, the second of four reaction wheels on the *Kepler* telescope failed, making it unable to continue observing the same field. In its two-wheel phase, called K2, the spacecraft can only reliably point at fields in the ecliptic plane for ~ 80 day long campaigns before it must turn to a new field to avoid the Sun. The *Kepler* spacecraft in its K2 mission continues to be a source of discovery for exoplanets (Howell et al. 2014).

joseph.schmitt@yale.edu

¹ Department of Astronomy, Yale University, New Haven, CT 06511 USA² Cerro Tololo Inter-American Observatory, Casilla 603, La Serena, Chile³ Department of Astronomy, California Institute of Technology, Pasadena, CA 91125, USA⁴ DTU Space, National Space Institute, Technical University of Denmark, Elektrovej 327, DK-2800 Lyngby, Denmark⁵ Planet Hunters citizen scientist⁶ Adler Planetarium, Department of Citizen Science, 1300 S Lake Shore Dr, Chicago, IL 60605⁷ Oxford Astrophysics, Denys Wilkinson Building, Keble Road, Oxford OX1 3RH⁸ CartoDB, 247 Centre Street, New York, NY 10013, USA⁹ Institute for Astronomy, Department of Physics, ETH Zurich, Wolfgang-Pauli-Strasse 27, CH-8093 Zurich, Switzerland¹⁰ <http://exoplanetarchive.ipac.caltech.edu>, last accessed February 25, 2016

Our target list consists of 75 stars observed by K2 during Campaigns 1-3. We conducted follow-up images of the 56 Campaign 1 (C1) targets and the two Campaign 2 (C2) targets at SOAR and observed the 17 Campaign 3 (C3) targets using Keck. The targets and their designations are listed in Table A1, which also lists the selection biases for each target. The URLs within Table A1 contain the GO proposal identifier as well as the full proposal for each target. The periods and epochs for all the EBs and EB candidates are listed in Table 1. The planet candidates are discussed more in Section 4.

2.1. Planet Hunters Targets

The citizen science project Planet Hunters¹¹ (PH, Fischer et al. 2012) was the primary source for finding 45 targets from C1 to C3. PH is a member of the citizen science Zooniverse¹² project (Lintott et al. 2008). PH volunteers organized their search on their own, surveying data from the K2 self-flat fielding (K2SFF) database (Vanderburg & Johnson 2014) or reducing the data themselves with the Guest Observer software PyKE (Still & Barclay 2012) or their own, self-created tools (e.g., LcTools¹³). Users check light curves for the signature of a planetary transit, EB, or other astrophysical objects (e.g., Kato & Osaki 2014). This project crowd-sources the analysis of K2 light curves and has been successful in the past in finding planet candidates (Fischer et al. 2012; Lintott et al. 2013; Wang et al. 2013; Schmitt et al. 2014a; Wang et al. 2015), confirming planets (Schwamb et al. 2013; Wang et al. 2013; Schmitt et al. 2014b), finding EBs (LaCourse et al. 2015), and finding other as of yet unidentified signals (Boyajian et al. 2015).

Among these 45 PH targets are WASP-85A b (Brown et al. 2014), which is a known exoplanet in a binary system, and nine other targets known to be EBs (eight from C1 and one from C3), according to the Guest Observer (GO) proposals requesting the targets. We have classified 10 of the 45 PH targets as Planet Hunter Objects of Interest (PHOIs), which is analogous to the Kepler Objects of Interest (KOI) designation. These were also discovered independently by Vanderburg et al. (2015). The rest of the PH targets are either previously known EBs or newly discovered candidate EBs, of which many were also independently found in Armstrong et al. (2015a).

2.2. Foreman-Mackey et al. (2015) Targets

Thirty of the C1 targets were selected from the K2 C1 planet candidate list by Foreman-Mackey et al. (2015), which comprises 36 planet candidates orbiting 31 stars. Several of these were also noted by PH volunteers. We selected all but one star, excluding EPIC 201565013 owing to its faintness, $K_P = 16.91$ mag. Of the 30 stars obtained from Foreman-Mackey et al. (2015), one of the targets, EPIC 201505350 (K2-19), was later con-

firmed to host a planet using ground-based photometric follow-up, transit timing analysis, AO imaging, spectroscopy, and photo-dynamical analysis (Armstrong et al. 2015b; Barros et al. 2015; Narita et al. 2015). Montet et al. (2015) later validated planets around 16 of these 30 stars, including the previously mentioned K2-19, using a statistical elimination of astrophysical false positives, while deeming six others to be likely false positives. EPIC 201465501 (K2-9) was also independently validated by Schlieder et al. (2016). We observed all 30 of these targets, regardless of their designation.

3. OBSERVATIONS AND DATA REDUCTION

On the nights of May 2-3, 2015, we observed 58 stars from the K2 program; 56 were from C1 and two were from C2. We used speckle interferometry with HRCAM (Tokovinin & Cantarutti 2008), a high resolution camera on the SOAR Adaptive Optics Module (SAM) at the 4.1-meter Southern Astrophysical Research (SOAR) telescope at Cerro Pachón Observatory. On the night of July 29, 2015, a portion of the night was devoted to observing the 17 stars from C3 with the NIRC2 instrument on the Keck II telescope.

3.1. SOAR speckle interferometry

For the 58 targets observed by SOAR, we used the Bessel *I*-band filter (central wavelength = 866.5 nm) on HRCAM because this provided better seeing and a wider bandwidth (FWHM = 391.4 nm) than in the visual and favored the detection of M-dwarf companion stars. Some time was lost because of clouds and technical problems. For both nights, the telescope was pointed directly into a strong wind. This buffeted the telescope and could cause high jitter up to 3".

For each target star, we typically took four data cubes with 400 images each. For the first two cubes, the field size was $6''.092 \times 6''.092$ using 200×200 binned (2×2) pixels with typical exposures of 200 ms. In the last two cubes, we did not bin the data. Correspondingly, the field size shrank to $3'' \times 3''$. The exposure times ranged between 20 and 50 ms for the smaller field. For the highest wind conditions, we only collected binned pixel data cubes. The wider fields allowed for the detection of fainter, more distant companions, while the narrow field cubes allow for the detection of brighter, closer companions. The detected companions have all been confirmed in multiple data cubes.

The data were processed using a standard speckle pipeline (Tokovinin et al. 2010). The pipeline delivered five products for each target: a power spectrum, an auto-correlation function computed from the power spectrum, an average image, an average image re-centered around the centroid, and a shift-and-add image re-centered on the brightest pixel. See Figure 1 for an example of each image product for EPIC 201555883. The detector orientation and pixel scale were accurately calibrated on wide binaries with well-modeled linear motions.

The faint magnitudes of our target stars required modifications to the standard pipeline. Hot pixels

¹¹ <http://www.planethunters.org/>

¹² <https://www.zooniverse.org/>

¹³ <https://dl.dropboxusercontent.com/u/78120543/LcTools/LcTools%20Product%20Description.html>

Table 1
EB and EBC properties.

EPIC ID	Campaign	Status	P_{PH} (days)	Epoch $_{\text{PH}}$ (KBJD ^a)	P_{KEB} (days)	Epoch $_{\text{KEB}}$ (KBJD)
201160662	C1	EBC	1.537	1975.957	1.53687 ± 0.00013	$1981.05912 \pm \dots$
201207683	C1	EBC	^b	2002.312	\dots	\dots
201246763	C1	EBC	43.663	2014.326	$43.66300 \pm \dots$	1962.93272 ± 0.57131
201253025 ^c	C1	EB	3.392	1980.767	6.78617 ± 0.00105	1978.12149 ± 0.03787
201270464 ^d	C1	EBC	3.155	1977.436	\dots	\dots
201324549 ^e	C1	EBC	2.519	1979.500	\dots	\dots
201407812	C1	EBC	2.827	1979.490	2.82678 ± 0.00030	1984.22530 ± 0.04365
201408204	C1	EB	8.482	2024.606	8.48191 ± 0.00137	2025.34343 ± 0.03497
201458798	C1	EBC	0.619	1977.568	0.61939 ± 0.00003	\dots
201488365	C1	EB	3.362	1975.859	3.36426 ± 0.00039	1981.44082 ± 0.04704
201567796	C1	EBC	5.011	1979.536	5.00861 ± 0.00069	2003.31875 ± 0.03142
201576812	C1	EB	5.730	1975.858	5.72823 ± 0.00084	1989.66917 ± 0.02229
201594823	C1	EB	1.301	1976.659	1.30062 ± 0.00010	1977.93351 ± 0.01931
201626686	C1	EBC	5.280	1979.356	5.28011 ± 0.00069	1973.08643 ± 0.03258
201648133	C1	EBC	35.020	1980.807	35.02000 ± 0.00735	$1972.47647 \pm \dots$
201665500	C1	EB	3.054	1977.539	3.05352 ± 0.00033	1990.67896 ± 0.03027
201704541	C1	EB	0.411	1976.547	0.41138 ± 0.00002	1975.24518 ± 0.02477
201705526	C1	EBC	18.103	1986.610	18.09409 ± 0.00381	$2012.62636 \pm \dots$
201711881	C1	EB	5.468	1977.988	5.46846 ± 0.00077	1975.43501 ± 0.30923
201725399	C1	EBC	2.162	1978.253	2.16127 ± 0.00020	1986.34269 ± 0.04807
201826968	C1	EBC	0.367	1976.608	0.36176 ± 0.00002	1974.23489 ± 0.03098
201890494	C1	EBC	2.536	1977.446	2.53657 ± 0.00026	1964.73129 ± 0.02028
201928968	C1	EBC	0.320	1980.390	0.32000 ± 0.00001	$1979.66097 \pm \dots$
203533312 ^f	C2	EBC	0.176	2061.640	\dots	\dots
204129699	C2	EBC	1.258	2060.600	1.25780 ± 0.00010	$2061.86700 \pm \dots$
205985357	C3	EBC	4.128	2148.728	\dots	\dots
206029314	C3	EBC	7.026	2148.069	\dots	\dots
206047297	C3	EBC	27.317	2166.457	\dots	\dots
206135075	C3	EBC	54.976	2149.868	\dots	\dots
206135267	C3	EB	2.533	2147.052	\dots	\dots
206152015	C3	EBC	0.809	2147.088	\dots	\dots
206173295	C3	EBC	2.176	2147.784	\dots	\dots
206311743	C3	EBC	4.312	2155.042	\dots	\dots
206380678 ^e	C3	EBC	2.271	2147.270	\dots	\dots

Note. — We list here the periods and epochs of the EBs and EB candidates both estimated by PH users, P_{PH} and Epoch $_{\text{PH}}$, and many of them also with data from a preliminary *Kepler* Eclipsing Binary catalog (Prša et al. 2011, K. Conroy 2015, private communication), P_{KEB} and Epoch $_{\text{KEB}}$.

^a *Kepler* Barycentric Julian Day (KBJD) is equal to JD minus 2454833.0 (UTC=January 1, 2009 12:00:00).

^b Single stellar eclipse (depth $\sim 24\%$).

^c PH users counted each transit as a primary transit, while the initial KEB catalog counted primary and secondary events. This explains the factor of two difference in the periods and the offset in the epoch.

^d Eclipse profile is shallow and V-shaped. May have alternating minima.

^e Eclipse profile is shallow and V-shaped.

^f The EB candidate may have $P_{\text{PH}} = 0.361$ days, double what is listed in the table.

from longer than standard exposures were fixed by removing the dark current and the bias and accounting for the 2x2 binning. Clock-injection charges (CICs) were a major contributor to the power spectrum of faint stars. CICs create a background of spurious photon spikes that bias the centroid of the star towards the middle of the frame, a problem for frames in which the star deviated far from the center, which occurred during periods of high wind. The CICs were removed by smoothing the images with a width of five pixels, taking its median-average as the background, and then subtracting it. A threshold of 0.3 times the maximum intensity above the background was also subtracted (and clipped at zero). This produces a properly centered image. To reduce the noise associated with CICs, we multiplied each re-centered image by a Gaussian mask of 15-pixel ($0''.46$) FWHM and calculated alternative power spectra from those masked images. Masking improved the signal-to-noise ratio in the

power spectrum, making closer companions more detectable at the expense of reducing detectability of companions beyond $0''.5$. Since high wind resulted in temporary losses of the image from the field of view (FOV), we removed frames if the centroid was calculated to be within 20 pixels of the frame border. For the shift-and-add method, if the brightest pixel was more than 20 pixels away from the centroid, the frame was removed as a likely cosmic ray event.

3.2. Keck AO imaging

We observed 17 K2 C3 planet candidates with the NIRC2 instrument at the Keck II telescope (Mauna Kea, Hawaii, United States). NIRC2 is a near infrared imager designed for the Keck AO system (Wizinowich et al. 2000). The observations were made on UT July 29, 2015, with $0''.8$ - $1''.0$ seeing. We selected the narrow camera mode, which has a pixel scale of 10 mas/pixel. The FOV is thus $10'' \times 10''$ for

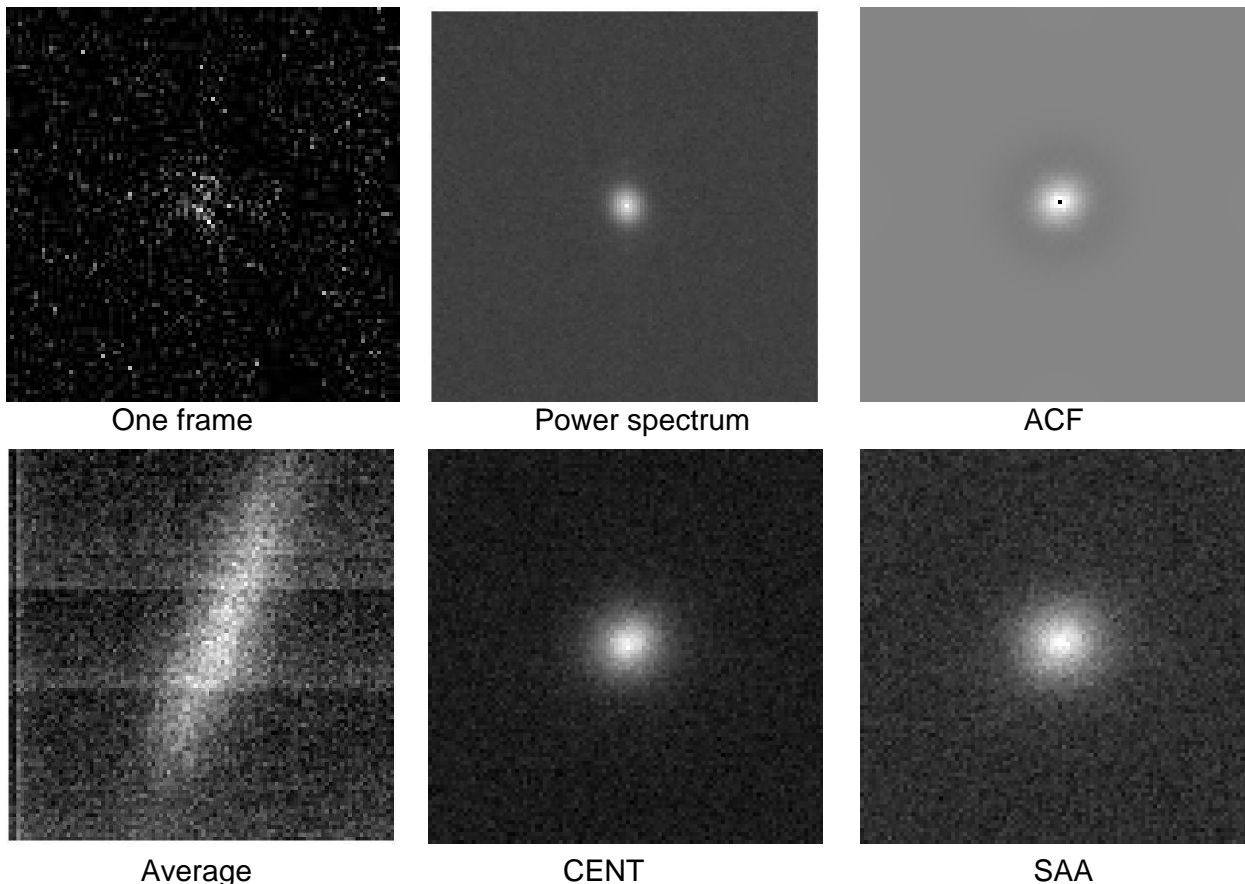


Figure 1. The various data products produced by the reduction pipeline for a single star (EPIC 201555883), i.e., a non-detection. The top left image is what a single frame in the analysis looks like, while the other five images show composites of all frames: the power spectrum, auto-correlation function (ACF), the average image, the average image re-centered around the centroid (CENT), and the shift-and-add method (SAA) of centering the image on the brightest pixel. The large jitter in the average image is caused by wind buffeting the telescope. The scale of each image is $6''.092 \times 6''.092$.

a mosaic $1K \times 1K$ detector. All images were taken in the K_s band, which provides higher sensitivity than J and H band for bound companions with late spectral type. Among the many sensors that allow the primary mirror segments to act as one mirror, an error in one of the sensors caused a co-phasing issue with about 25% of the mirror segments. The Keck team hopes to implement better alarms on the primary mirror to alert them to similar mirror-induced image quality problems (J. Lyke 2016, private communication). This degraded our AO-corrected point spread function and decreased our performance relative to standard NIRC2 observations. Exposure time was set such that the peak flux of the target was at least 5,000 ADU after co-add. Before co-add, peak flux was limited to 2,000 ADU to avoid non-linearity and detector persistence. We used a 3-point dither pattern (three corners of a square) with a throw of $2''.5$. We avoided the lower left quadrant in the dither pattern because it has a much higher instrumental noise than the other three quadrants on the detector.

The raw Keck NIRC2 AO data were processed using standard techniques to replace bad pixels, subtract dark frames, flat-field, subtract sky background, and align and co-add frames. Our own custom program recorded the differential magnitude,

separation, position angle (θ), and detection significance. All detections were then visually checked to remove confusions such as speckles, background extended sources, and cosmic ray hits.

4. TRANSIT FITTING FOR PHOIS

For each of the PHOIs listed in Table 2, we downloaded the K2SFF light curves from (Vanderburg & Johnson 2014). The K2SFF data reduction process removes the effect of the spacecraft thruster fires that occur approximately every six hours, although it does not do so perfectly in all cases. The K2SFF reduction process is not intended to remove stellar variations. We flattened these K2SFF light curves with low-order ($n \leq 4$) polynomial fits to out-of-transit data and clipped the light curves around the transits using a combination of our own codes, the aforementioned PyKE software, and the IDL program `autoKep` (Gazak et al. 2012). One occasional side effect of the K2SFF reduction process was a ringing-like signature in the location where a transit should have been. These affected transits were typically removed from our analysis. However, in the three-transit case of EPIC 206155547, we extracted one of these badly reduced transits from the raw data since there was no apparent data discontinuity caused by a thruster fire during the transit. We then fit the raw, out-of-transit

data on either side of the transit to a quadratic polynomial and removed the trend in a similar manner as the flattening of the K2SFF light curves. Another common effect was a spike in brightness within transits, which typically degraded the transit to such a degree that the transit was simply removed from analysis. One exception is the brightness spike in the first transit of EPIC 201516974. Due to its longer period ($P = 36.7$ d) and thus longer duration, the spike degraded only a minority of the transit. Therefore, we simply masked the spike out (partially shown in gray squares in Figure 2).

Some of the PHOIs have suspected signals of stellar activity, either from large-scale brightness variations in the overall light curve or from bumps within the transit. For EPIC 206432863, we masked out two suspected starspot crossings (shown in gray in Figure 2). For other stars, there were no sharp, clearly defined starspot or plage crossings, but small-scale stellar activity was evident in the increased scatter in the in-transit residuals of some of the fits.

The transit parameters were fit by the IDL program TAP (Gazak et al. 2012), an MCMC fitting routine using EXOFAST (Eastman et al. 2013) to calculate Mandel & Agol (2002) transit models using a wavelet-based likelihood function (Carter & Winn 2009). TAP was used to fit the impact parameter b , the transit duration T , the ratio of the planet radius to the stellar radius R_P/R_* , the midtransit times, linear and quadratic limb darkening, red and white noise, and the coefficients of a quadratic normalization polynomial for each individual transit event (in case of an imperfectly normalized or flattened light curve). The ratio of the semi-major axis to the stellar radius a/R_* and the inclination i were derived from the posterior of each solution by TAP using T and b . Circular orbits were assumed. Each set of transits were fit with ten MCMC chains of various lengths (100,000-2,000,000) to ensure no indication of non-convergence according to the Gelman-Rubin statistic (Gelman & Rubin 1992). The period P is poorly constrained by TAP. Therefore, for each PHOI, we randomly drew 1,000,000 samples of each individual transit’s midpoint from the TAP posterior and calculated the period between consecutive fitted transits, taking into account missing transits where necessary. We then took the median and its 1σ upper and lower error bars. The transits and their fits are shown in Figures 2.

One important caveat to the numbers in Table 2 and the best-fit lines in Figure 2 is that we have chosen to present the median values and their 1σ error bars as they better capture the distribution of each parameter. However, the median value is not necessarily the most likely model. Transit light curve fitting can result in bimodal distributions due to weak degeneracies between the parameters, such as T and b . More often than not, the effect is minor, and the median value closely approximates the most likely value for the most important physical parameters, such as R_P/R_* . However, there are cases where the most likely value is moderately different from the

median, even being at the edge of the 1σ error bars in the more extreme cases. In Figure 2, this causes the structure one sees in the residual to the median model. One specific example of this effect is the fit for EPIC 206082454 (PHOI-6 b). The median value of R_P/R_* is actually a local minimum. For this planet, the upper and lower 1σ limit closely approximates the center of the two local maxima. This has the effect in Figure 2 of placing the fit line below most of the data points in the bottom of the transit. The same applies for EPIC 206245553 (PHOI-8 b). For both stars, a/R_* and i also show a bimodal distribution. To qualitatively show the agreement (or disagreement) between the median model and the single most likely individual model, we also plot the most likely single model from the MCMC analysis in yellow.

5. RESULTS

5.1. Previously known binaries

For all 75 targets, we searched the literature for companions within our FOV. Our search included several surveys and catalogs: APASS (Henden & Munari 2014), SDSS (Alam et al. 2015), 2MASS (Skrutskie et al. 2006), WISE (Wright et al. 2010), and the Washington Double Star (WDS) catalog (Mason et al. 2001). Many of the potential companions were low signal to noise, had aberrations caused by diffraction spikes (particularly in SDSS), or were otherwise unlikely to be true stars. We performed a manual triage to include only high quality detections of companion stars. Unfortunately, however, the two C2 targets and 11 of the 17 C3 targets have not been observed by SDSS. We identified four known companions in the literature search, one in SDSS (EPIC 201890494), one in the WDS catalog (EPIC 201862715), and two in Montet et al. (2015, EPIC 201546283 and EPIC 201828749).

The companion to EPIC 201890494 found by SDSS was successfully recovered. We also recovered the companion to EPIC 201862715 (WASP-85). This is a visual, G-K dwarf binary system (Burnham 1882) listed in the WDS catalog. The primary component hosts an inflated hot Jupiter, named WASP-85A b, which was confirmed via ground-based photometry, radial velocities, and K2 photometry (Brown et al. 2014).

The two other stars known to have companions were discovered by Montet et al. (2015), who observed seven of the candidates in Foreman-Mackey et al. (2015) with the Palomar High Angular Resolution Observer (PHARO) infrared detector (Hayward et al. 2001) AO system (Dekany et al. 2013) at the 5.1 meter Palomar Hale telescope. The two of their targets that resulted in a detection of a nearby companion star were EPIC 201546283 and EPIC 201828749. We recovered only the latter companion, which was originally measured to have $\rho = 2''.46 \pm 0''.04$ and $\Delta m_J = 1.462 \pm 0.012$ mag (B. Montet 2015, private communication). The unrecovered companion was likely missed due to the combination

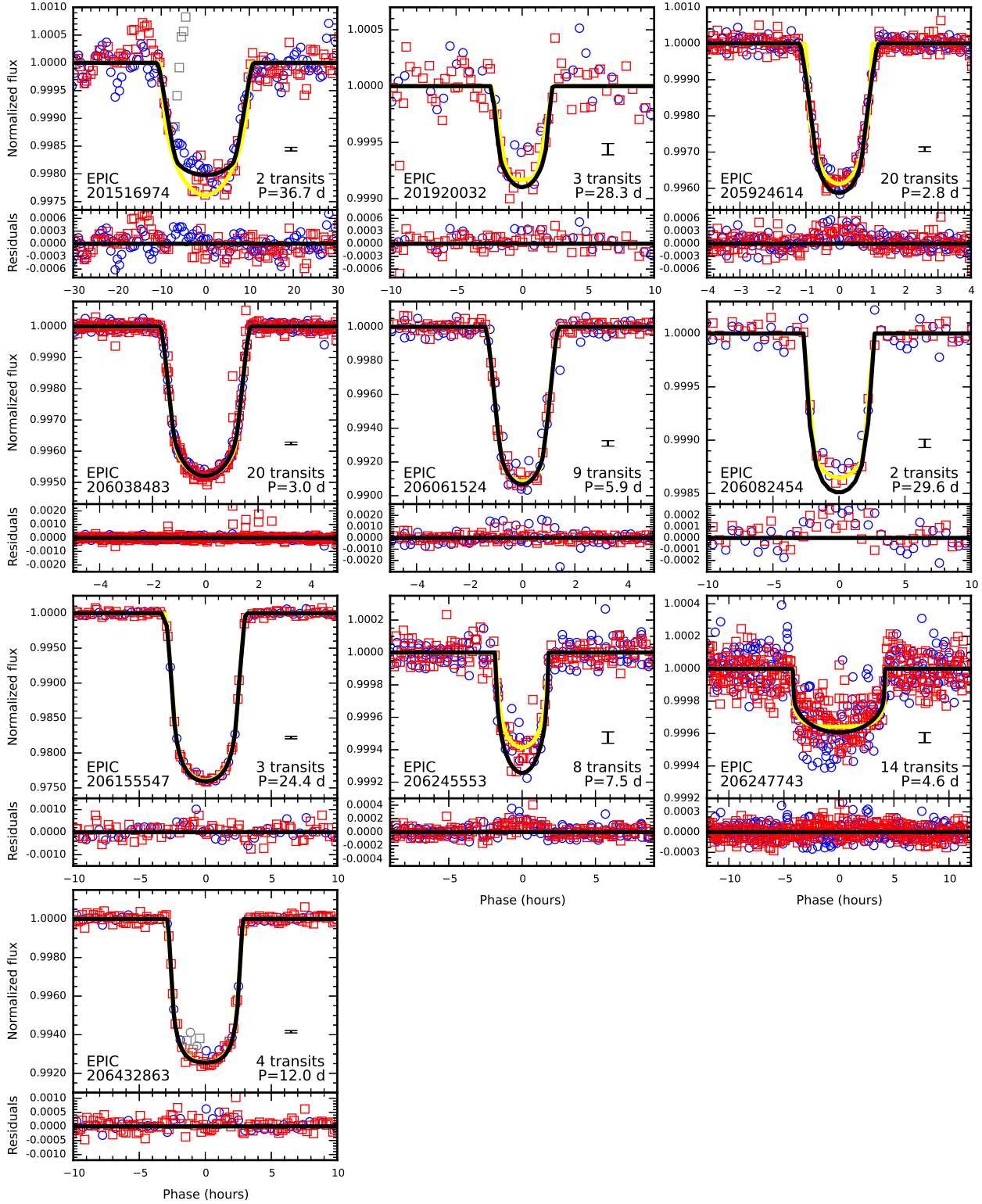


Figure 2. Top panels are the transit fits for all PHOIs. Odd-numbered transits (one-based indexing) are shown in red squares, while even-numbered transits are shown in blue circles. The solid, black line is the median model fit, while the most likely individual model from the MCMC analysis is highlighted in yellow. Visible differences between these two fit lines are caused by the bimodality of the MCMC results. A representative error bar ($\pm\sigma$) is shown in black in the bottom right of each panel above the label for number of transits. Grayed squares for EPIC 201516974 represent data points masked due to detrending issues, while grayed circles and squares for EPIC 206432863 represent data points masked due to suspected starspot crossings. Bottom panels display the residuals of the data minus the median model. Comparing to the median model results in some structure in the residuals when there is a significant difference between the median model and the most likely model.

Table 2
PHOI transit fit results and derived parameters.

EPIC ID	PHOI ID ^a	P (days)	Epoch (KBJD ^b)	T (hours)	b	R_P/R_*	a/R_*	i (deg)
201516974	1 b	36.7099 ^{+0.0124} _{-0.0126}	1986.8056 ^{+0.0098} _{-0.0095}	0.736 ^{+0.070} _{-0.039}	0.90 ^{+0.03} _{-0.12}	0.0489 ^{+0.0028} _{-0.0033}	6.9 ^{+2.2} _{-0.7}	82.6 ^{+2.5} _{-1.1}
201920032	2 b	28.2717 ^{+0.0141} _{-0.0139}	2000.2058 ^{+0.0051} _{-0.0059}	0.171 ^{+0.011} _{-0.010}	0.01 ^{+0.74} _{-0.75}	0.0264 ^{+0.0047} _{-0.0020}	42.8 ^{+8.2} _{-18.3}	89.3 ^{+0.5} _{-1.3}
205924614	3 b	2.8493 ^{+0.0013} _{-0.0015}	2150.4245 ^{+0.0008} _{-0.0008}	0.078 ^{+0.001} _{-0.002}	0.14 ^{+0.49} _{-0.61}	0.0574 ^{+0.0032} _{-0.0019}	10.1 ^{+1.8} _{-1.6}	87.5 ^{+1.7} _{-2.0}
206038483	4 b	3.0026 ^{+0.0012} _{-0.0012}	2149.0598 ^{+0.0005} _{-0.0005}	0.120 ^{+0.001} _{-0.001}	0.80 ^{+0.01} _{-0.02}	0.0696 ^{+0.0010} _{-0.0008}	4.9 ^{+0.5} _{-0.5}	80.6 ^{+0.9} _{-1.2}
206061524	5 b	5.8797 ^{+0.0018} _{-0.0015}	2153.3239 ^{+0.0006} _{-0.0006}	0.093 ^{+0.003} _{-0.003}	0.80 ^{+0.03} _{-0.03}	0.0982 ^{+0.0024} _{-0.0020}	12.1 ^{+0.9} _{-0.8}	86.2 ^{+0.4} _{-0.4}
206082454	6 b	29.6260 ^{+0.0016} _{-0.0017}	2160.5402 ^{+0.0011} _{-0.0011}	0.194 ^{+0.006} _{-0.004}	0.09 ^{+0.74} _{-0.86}	0.0348 ^{+0.0036} _{-0.0022}	36.8 ^{+9.9} _{-11.9}	89.0 ^{+0.7} _{-1.0}
206155547	7 b	24.3872 ^{+0.0010} _{-0.0012}	2152.8841 ^{+0.0002} _{-0.0002}	0.226 ^{+0.001} _{-0.002}	0.29 ^{+0.07} _{-0.63}	0.1401 ^{+0.0014} _{-0.0013}	32.4 ^{+0.6} _{-0.6}	89.4 ^{+0.1} _{-0.1}
206245553	8 b	7.4950 ^{+0.0084} _{-0.0069}	2154.6728 ^{+0.0013} _{-0.0018}	0.147 ^{+0.003} _{-0.005}	0.28 ^{+0.57} _{-1.01}	0.0239 ^{+0.0035} _{-0.0021}	11.8 ^{+3.6} _{-3.7}	86.7 ^{+2.4} _{-2.9}
206247743	9 b	4.6028 ^{+0.0342} _{-0.0289}	2147.8210 ^{+0.0047} _{-0.0041}	0.341 ^{+0.008} _{-0.009}	0.04 ^{+0.62} _{-0.55}	0.0178 ^{+0.0012} _{-0.0006}	3.8 ^{+0.5} _{-0.7}	83.4 ^{+4.6} _{-6.9}
206432863	10 b	11.9897 ^{+0.0008} _{-0.0012}	2150.8263 ^{+0.0005} _{-0.0005}	0.223 ^{+0.001} _{-0.002}	0.29 ^{+0.22} _{-0.78}	0.0787 ^{+0.0010} _{-0.0011}	15.1 ^{+0.8} _{-0.7}	88.2 ^{+0.4} _{-0.3}

Note. — For definitions of each parameter, see Section 4. These are the median and 1σ values from the TAP fits, which are not necessarily the best fit models. See Section 4 for a

^a Full PC names are PHOI-1 b, PHOI-2 b, etc.

^b *Kepler* Barycentric Julian Day (KBJD) is equal to JD minus 2454833.0 (UTC=January 1, 2009 12:00:00).

of the companion’s distance from the primary ($\rho = 2''.98 \pm 0''.05$), putting it at the edge of our detector, and its faintness ($\Delta m_{K_s} = 3.72$ mag, B. Montet 2015, private communication), which implies a higher Δm_I close to our detection limit of $\Delta m_I = 5.0$ at $> 2''$ for this star.

All three companions recovered were found with the SOAR observations. See Table 3 for their properties and Figure 3 for images of the companions. These images are for illustrative value only and were not used to make the discovery. Each companion was found independently in multiple data cubes.

5.2. New Detections

We detected three new companions with the SOAR observations (see Table 3). From the SOAR observations, we did not discover any new stellar companions among the planet candidates. Of the eight known EBs, one new companion was discovered (EPIC 201704541). Around the 17 EB candidates, two new companion stars were discovered near EPIC 201324549 and EPIC 201826968. See Figure 3 for speckle images of the companions. Again, these images are for illustrative value only. Each new companion was found in multiple data cubes.

We also detected three new companions with the Keck observations (again, Table 3). From the Keck AO imaging, all three newly discovered companions are within $1''$ of the primary star. One companion was near one of the PHOs (EPIC 206061524), one was near the EB (EPIC 206135267), and one was near an EB candidate (EPIC 206152015). See Figure 4 for the AO detection images.

5.3. Non-detections

We discovered companion stars for only 12% of our targets. However, non-detections are as important as detections in determining multiplicity rates. Due to distortions when measuring detection limits around binaries, we place detection limits only on the non-detections. We estimated detection limits by the standard technique of calculating root-mean-square intensity fluctuations, σ , in annular zones of increasing radii and assumed that a companion with a central intensity of 5σ would be detectable. For the SOAR non-detections, we also verified detection limits by simulating ≈ 100 companions near the expected 5σ detection curve for each star and attempting to recover them, typically validating the 5σ initial estimate for the detection curve, although it appeared to be a slightly conservative estimate. Overall, the detection curves are more accurate at larger separations as the area of the annulus becomes larger. The deeper, binned exposures gave better detections at large separations up to $3''$.

Table 4 and Figure 5 show the detection curves for all 66 stars with no detections. Figure 5 also shows the median detection curve and the separations and Δm ’s for all detections from both instruments, both previously known and newly discovered. Five of the companions are at sub-arcsecond separations.

5.4. Physical association of the detected companions

Detected companions may be either physically bound to the primary star or may be a foreground or background star. We tested the probability that any of our detections could be the result of a chance alignment with a non-physically associated star. We used the TRILEGAL Galactic population model (Girardi et al. 2005) to simulate a one square degree Galactic population of stars in the direction of each target with a detected companion and created nine simulated fields, one for each star with a companion. We assumed that the distribution over this one square degree was uniform. All of our detected companion stars from SOAR are brighter than $m_I = 15.0$ mag, and all of our detected companion stars from Keck are brighter than $m_{K_s} = 16.0$ mag, so we counted the number of brighter stars in each respective field (i.e., brighter than $m_I = 15.0$ mag for SOAR fields and brighter than $m_{K_s} = 16.0$ mag for Keck fields). We then divided that number of stars by one square degree to get a surface density of stars and then multiplied by our FOV to determine the probability that any of these stars would be within our FOV. For the nine stars, the probability of chance projection within $3''$ of the primary ranges between 0.07% and 0.5%. The probabilities are even lower when considering separations less than or equal to the measured companion separations rather than the entire $3''$ range (see Table 3), strongly suggesting that all detected companions at these high Galactic latitudes are physically associated with their respective primaries.

6. DISCUSSION

High resolution imaging is particularly important for exoplanets studies. If a companion star is detected, it means that the signal from the planet is diluted and that the true planet radius is larger than initially measured. The magnitude of this increase depends on the relative brightness of the two stars and knowledge of which star the planet orbits. If the two stars are of near equal brightness, the true planet radius will be about half that which was measured. For binaries with a large Δm , the true planet radius will either be nearly the same as the measured value (if the planet orbits the primary star), or the true planet radius will be greatly increased (if the planet orbits the secondary star). A good example of correcting for the dilution caused by a companion star is shown in Dressing et al. (2014). The average planetary radius from transit surveys may be underestimated by a factor of 1.5, although this can be reduced to 1.2 with radial velocity and high resolution data (Ciardi et al. 2015).

These data are also useful for the statistical validation of planet candidates. Both detections and non-detections with contrast curves can provide sufficient constraints to rule out enough parameter space from astrophysical false positives to statistically validate the planet candidate as a true planet. This has been done for many planets with the BLENDER code (e.g., Torres et al. 2011).

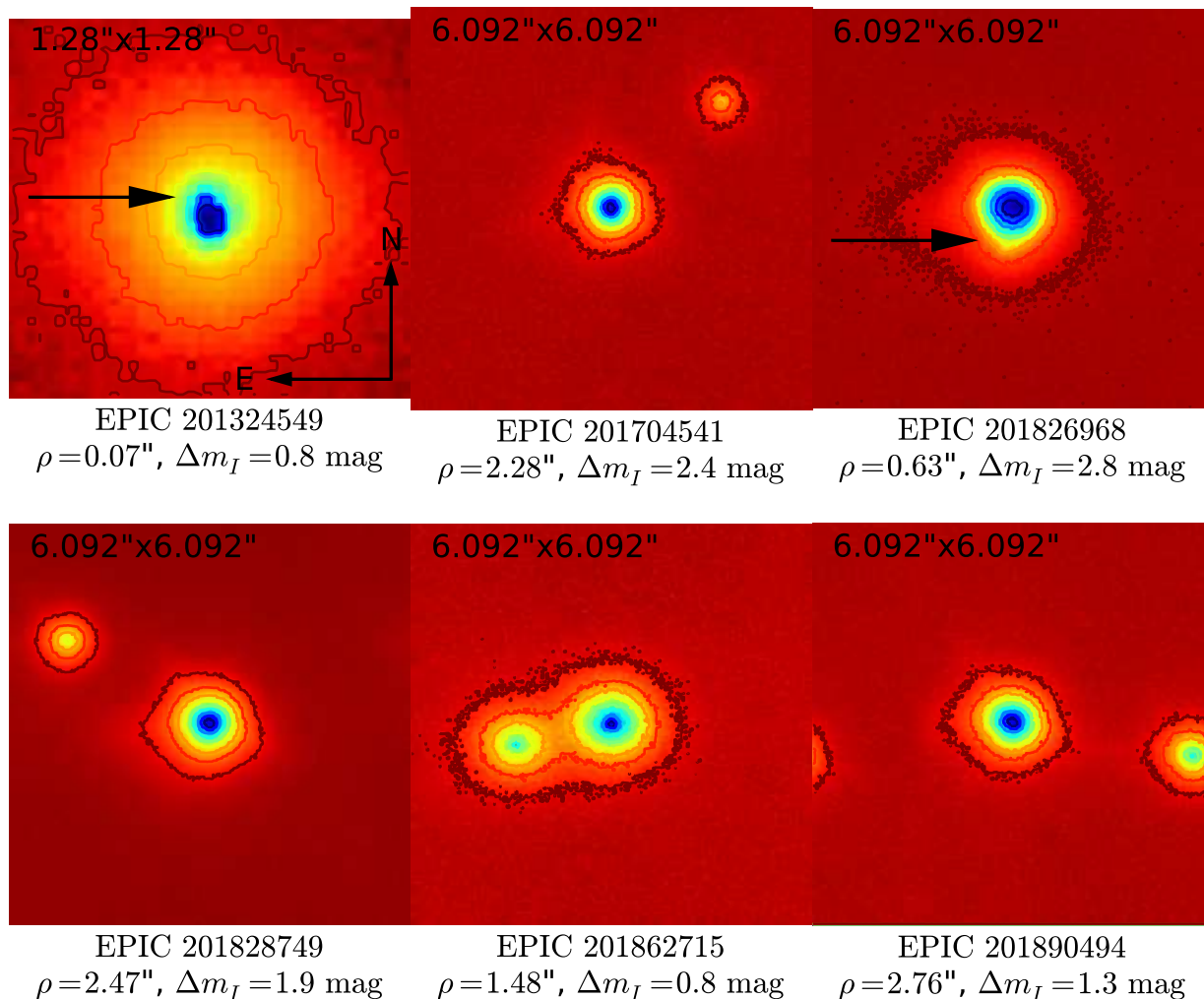


Figure 3. The binaries detected by SOAR speckle interferometry. Arrows point to the sub-arcsecond detections. The companion to EPIC 201324549 can be seen in the blue bump to the north-northeast, while the companion to EPIC 201826968 can be seen as the yellow bump south of EPIC 201826968. These images are for illustrative value only. They were not used to make the discovery. Each companion was independently detected in multiple data cubes.

Recently, studies have also attempted to determine the relationship between stellar multiplicity and exoplanets. The multiplicity rate of known exoplanet hosts compared to stars not known to host planets can inform our knowledge of planet formation¹⁴. If exoplanets are more frequently found in multiple star systems, one can assume that multiplicity enhances planet formation. If exoplanets are found to be less common in multiple star systems, one can conversely assume that multiplicity suppresses planet formation. Studies differ on whether the multiplicity rate of known exoplanet host stars is consistent with the multiplicity rate of stars without known exoplanets (Bonavita & Desidera 2007; Raghavan et al. 2010; Lodieu et al. 2014) or whether the multiplicity rate of known exoplanet host stars is lower (Mugrauer & Neuhäuser 2009; Roell et al. 2012; Wang et al. 2014). The existence

¹⁴ One must be careful not to say “known non-exoplanet host stars”, as it is currently impossible to prove that any one star does not host any planet. Rather, one usually compares known exoplanet host stars to stars known not to host stars above some detectable threshold or to field stars, some of which will host undiscovered exoplanets.

of companion stars may also influence the architecture of planetary system (e.g., Quintana et al. 2007; Desidera & Barbieri 2007; Roell et al. 2012), although some studies have put constraints on their potential influence, such as no correlation existing between misaligned or eccentric hot Jupiters and the incidence of directly imaged stellar companions (e.g., Ngo et al. 2015).

7. CONCLUSIONS

We found nine companion stars within $3''$ of three candidate transiting exoplanet host stars and six EB candidates. All nine companion stars are likely to be physically associated with the target star. Six of the nine detected companions are new discoveries, five of them associated with likely EBs.

Without knowledge of the physical binary separations, it is difficult to determine whether or not there are any potentially significant deviations between the binary statistics in any sub-sample of our target stars and the binary statistics of the population of field stars. However, it is worth noting that many of the short-period EBs and EB candidates ($P < 3$ days) were found to have compan-

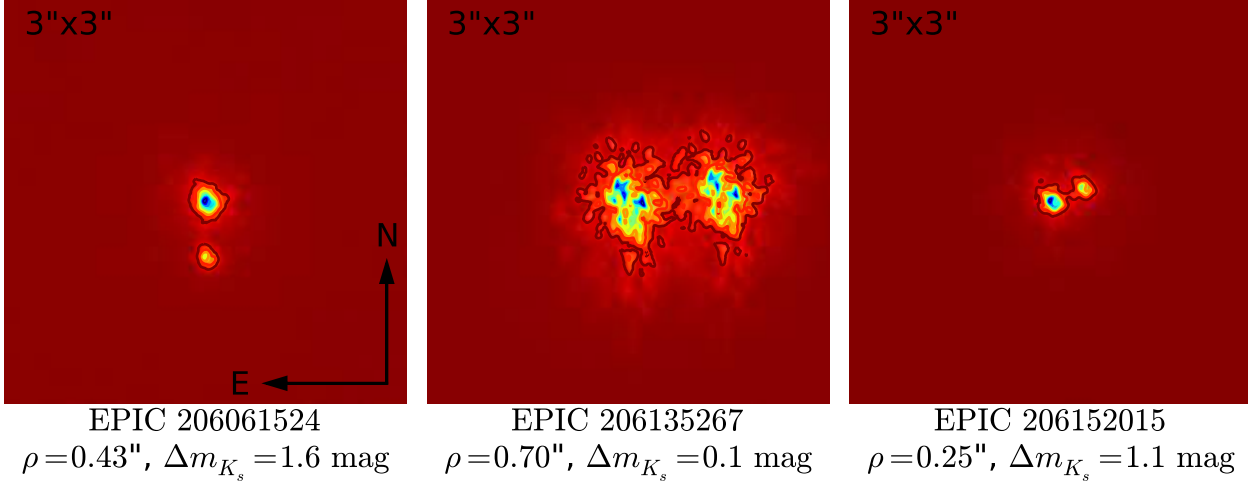


Figure 4. The binaries detected by Keck NIRC2 AO imaging. Due to the close separation of the two stars for EPIC 206135267 and their near equal brightness, the AO corrections system became confused, and the AO correction has been much reduced.

Table 3
Binary detections.

EPIC ID	Status	First detection	Epoch +2000	θ (degrees)	$\rho\sigma_\theta$ ^a (mas)	ρ (")	$\sigma\rho$ (mas)	Δm ^b (mag)	Prob. Proj. ^c (%)
201324549	EBC	This paper (SOAR speckle)	15.3380	12.2	3.9	0.0721	4.4	0.8	0.00039
201704541	EB	This paper (SOAR speckle)	15.3380	310.8	4.9	2.2793	4.9	2.4	0.041
201826968	EBC	This paper (SOAR speckle)	15.3379	164.7	13.3	0.6330	6.7	2.8	0.041
201828749	PC	Montet et al. (2015)	15.3353	57.2	0.7	2.4684	0.7	1.9	0.24
201862715	CP	Burnham (1882)	15.3350	99.7	0.4	1.4786	0.4	0.8	0.062
201890494	EBC	SDSS	15.3379	256.6	1.3	2.7597	1.3	1.3	0.071
206061524	PHOI	This paper (Keck AO)	...	179.3	3.8	0.43	10	1.6	0.0035
206135267	EB	This paper (Keck AO)	...	279.9	6.1	0.70	10	0.1	0.0088
206152015	EBC	This paper (Keck AO)	...	291.4	2.2	0.25	10	1.1	0.0011

Note. — The error on Δm is 0.1 mag.

^a The tangential error.

^b For SOAR detections $\Delta m = \Delta m_I$. For Keck detections, $\Delta m = \Delta m_{K_s}$.

^c This is the probability that projection effects could place an unbound background or foreground star at an angular separation less than or equal the measured separation. See Section 5.4 for more details.

ions, supporting the conclusions in Tokovinin et al. (2006) that all short-period ($P < 3$ days) EBs have wider companions. These observations contribute to the growing dataset describing the multiplicity of our galactic neighborhood. This will soon help shed light on the influence that stellar multiplicity might have on planet formation.

Acknowledgements

JRS and TSB acknowledge support from NASA ADAP 14-0245. DAF acknowledges funding support for Planet Hunters from Yale University and acknowledges support from NASA ADAP12-0172. TSB acknowledges funding support from 14-K2GO1.2-0075, 14-K2GO2.2-0075, and 15-K2GO3.2-0063. KS gratefully acknowledges support from Swiss National Science Foundation Grant PP00P2_138979/1. The Zooniverse is supported by The Leverhulme Trust and by the Alfred P. Sloan foundation. PH is supported in part by NASA JPL's PlanetQuest program. The data presented in this paper are the result of the efforts of the PH volunteers, without whom this work would not have been possible. Their

contributions are individually acknowledged at <http://www.planethunters.org/authors>. The authors thank the PH volunteers who participated in identifying and analyzing the planet and EB candidates presented in this paper. The authors also thank Andrew Vanderburg and the Harvard-Smithsonian Center for Astrophysics for making available the reduced light curves for K2 C1, C2, and C3.

Some of the research presented in this paper is based on observations obtained at the Southern Astrophysical Research (SOAR) telescope, which is a joint project of the Ministério da Ciência, Tecnologia, e Inovação (MCTI) da República Federativa do Brasil, the U.S. National Optical Astronomy Observatory (NOAO), the University of North Carolina at Chapel Hill (UNC), and Michigan State University (MSU). Some of the data presented herein were obtained at the W. M. Keck Observatory, which is operated as a scientific partnership among the California Institute of Technology, the University of California and the National Aeronautics and Space Administration. The Observatory was made possible by the generous financial support of the W. M.

Table 4
Detection limits of the 52 stars with no detections.

EPIC ID	Telescope	Min. Sep. ^a (mas)	$\Delta m(0.25'')$ (mag)	$\Delta m(0.50'')$ (mag)	$\Delta m(1.00'')$ (mag)	$\Delta m(2.00'')$ (mag)
201160662	SOAR	0.14	2.70	4.06	5.08	5.57
201207683	SOAR	0.13	3.15	3.96	5.03	6.15
201208431	SOAR	0.12	2.36	3.44	4.43	4.55
201246763	SOAR	0.13	1.93	2.97	4.26	5.01
201253025	SOAR	0.18	2.02	2.89	4.08	4.70
201257461	SOAR	0.11	2.46	3.45	4.62	5.73
201270464	SOAR	0.08	2.15	2.38	3.04	4.50
201295312	SOAR	0.11	2.45	3.84	5.22	5.94
201338508	SOAR	0.15	2.23	3.15	4.01	4.25
201367065	SOAR	0.11	2.58	3.78	5.05	6.44
201384232	SOAR	0.14	2.24	2.87	4.36	5.33
201393098	SOAR	0.17	2.01	3.08	4.64	4.99
201403446	SOAR	0.11	2.77	3.76	5.29	6.01
201407812	SOAR	0.14	2.92	3.87	4.83	5.27
201408204	SOAR	0.13	2.84	3.93	4.61	4.99
201445392	SOAR	0.17	2.32	3.00	3.78	3.86
201458798	SOAR	0.14	2.87	3.99	4.70	4.97
201465501	SOAR	0.13	2.35	3.46	4.33	4.34
201488365	SOAR	0.11	1.46	1.84	3.37	4.19
201505350	SOAR	0.10	2.50	3.73	5.07	5.35
201516974	SOAR	0.13	2.64	3.51	4.97	6.38
201546283	SOAR	0.16	2.64	2.99	3.98	5.00
201549860	SOAR	0.12	2.24	3.57	4.82	4.89
201555883	SOAR	0.14	2.05	2.78	3.54	3.60
201567796	SOAR	0.11	2.21	3.83	4.43	6.34
201569483	SOAR	0.12	2.34	3.06	4.61	5.53
201576812	SOAR	0.11	2.21	2.32	3.91	4.88
201577035	SOAR	0.12	2.32	3.49	4.28	5.54
201594823	SOAR	0.14	2.84	3.80	4.70	5.40
201596316	SOAR	0.13	2.19	3.40	4.99	5.27
201613023	SOAR	0.18	1.90	2.80	4.16	5.47
201617985	SOAR	0.18	2.23	2.97	4.02	4.39
201626686	SOAR	0.18	1.88	3.37	4.86	5.72
201629650	SOAR	0.13	2.45	3.38	5.27	5.77
201635569	SOAR	0.19	2.05	2.64	3.21	3.36
201648133	SOAR	0.12	3.18	3.92	4.91	5.86
201649426	SOAR	0.16	2.27	3.36	4.72	5.35
201665500	SOAR	0.14	2.37	3.04	4.29	4.83
201702477	SOAR	0.18	1.92	2.71	3.42	3.47
201705526	SOAR	0.11	2.93	3.81	4.63	5.89
201711881	SOAR	0.11	2.27	3.32	4.55	5.38
201725399	SOAR	0.16	1.70	3.01	4.10	4.48
201736247	SOAR	0.10	1.72	2.59	3.11	3.31
201754305	SOAR	0.17	1.87	2.54	3.38	3.55
201779067	SOAR	0.11	2.59	3.25	4.40	6.55
201855371	SOAR	0.19	1.83	2.62	3.98	5.03
201912552	SOAR	0.10	2.62	3.53	4.25	5.81
201920032	SOAR	0.12	2.03	3.04	4.53	5.21
201928968	SOAR	0.08	2.91	3.73	4.17	5.68
201929294	SOAR	0.21	1.67	2.44	3.81	4.49
203533312	SOAR	0.13	2.01	2.76	3.51	4.52
204129699	SOAR	0.09	2.44	3.15	4.11	4.96
205924614	Keck	0.06	4.00	5.47	6.03	6.07
205985357	Keck	0.06	3.77	4.86	5.19	5.23
206029314	Keck	0.06	4.06	5.15	5.47	5.49
206038483	Keck	0.06	4.02	5.53	6.20	6.25
206047297	Keck	0.07	3.46	5.04	6.35	6.58
206082454	Keck	0.06	3.60	5.28	6.21	6.30
206135075	Keck	0.06	3.51	5.15	6.07	6.19
206155547	Keck	0.06	3.21	4.25	4.57	4.63
206173295	Keck	0.06	3.51	5.10	5.86	5.95
206245553	Keck	0.06	3.44	5.19	6.43	6.59
206247743	Keck	0.06	3.53	5.21	6.64	6.94
206311743	Keck	0.06	3.55	5.33	6.15	6.29
206380678	Keck	0.07	3.44	4.54	4.94	5.05
206432863	Keck	0.06	3.52	4.70	5.27	5.33

Note. — Δm limits at 0.25'', 0.50'', 1.00'', and 2.00''. Beyond 2.00'', the detection limits remain constant. The SOAR observations were taken in the I band, and the Keck observations were imaged in the K_s band.

^a Minimum separation, approximately the distance at which a companion star with $\Delta m = 0$ would be detectable.

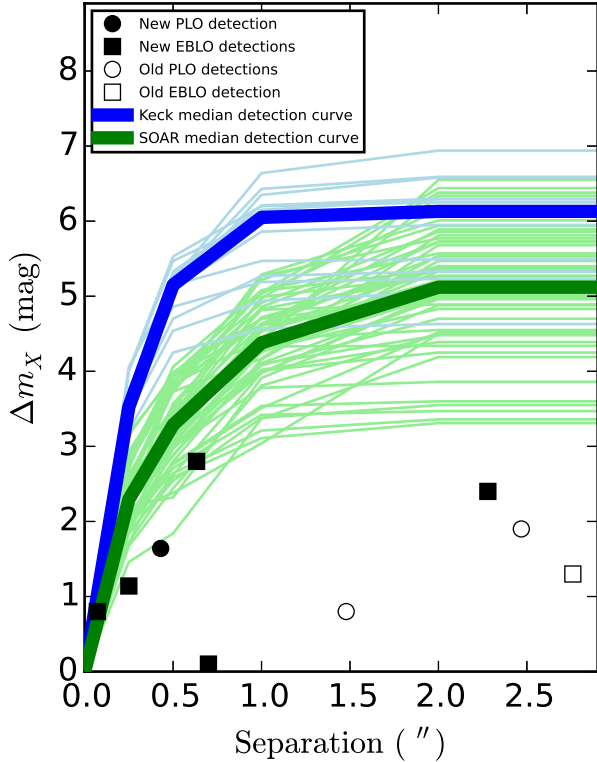


Figure 5. Detection curve for every star with no detections using data from Table 4. Light blue lines are for Keck AO (K_s -band), and light green lines are for SOAR speckle interferometry (I -band). The median of all detection curves from each telescope is highlighted with a thicker, darker line (top thick line for Keck, bottom thick line for SOAR). Circles denote companions near planet-like objects (PLOs), and squares denote companions near EB-like objects (EBLOs). Empty symbols are previously known companions, while filled circles are newly discovered companions. Companion stars below the detection curve were likely to be detected, while those above were unlikely to be detected.

Keck Foundation.

This paper includes data collected by the *Kepler* spacecraft, and we gratefully acknowledge the entire *Kepler* mission team's efforts in obtaining and providing the light curves used in this analysis. Funding for the *Kepler* mission is provided by the NASA Science Mission directorate. Support for MAST for non-HST data is provided by the NASA Office of Space Science via grant NNX13AC07G and by other grants and contracts. This research has made use of NASA's Astrophysics Data System Bibliographic Services, the Washington Double Star Catalog maintained at the U.S. Naval Observatory, and the APASS database, located at the AAVSO web site. Funding for APASS has been provided by the Robert Martin Ayers Sciences Fund. This publication makes use of data products from the Two Micron All Sky Survey, which is a joint project of the University of Massachusetts and the Infrared Processing and Analysis Center/California Institute of Technology, funded by the National Aeronautics and Space Administration and the National Science Foundation. Funding for the Sloan Digital Sky Survey IV has been provided by the Alfred P. Sloan Foundation, the U.S. Department of Energy Office of Science, and the Participating In-

stitutions. SDSS- IV acknowledges support and resources from the Center for High-Performance Computing at the University of Utah. The SDSS web site is www.sdss.org. This publication makes use of data products from the Wide-field Infrared Survey Explorer, which is a joint project of the University of California, Los Angeles, and the Jet Propulsion Laboratory/California Institute of Technology, funded by the National Aeronautics and Space Administration.

REFERENCES

- Abt, H. A., & Levy, S. G. 1976, *ApJS*, 30, 273
 Alam, S., Albareti, F. D., Allende Prieto, C., et al. 2015, *ApJS*, 219, 12
 Armstrong, D. J., Kirk, J., Lam, K. W. F., et al. 2015a, *ArXiv e-prints*, arXiv:1512.01246
 Armstrong, D. J., Santerne, A., Veras, D., et al. 2015b, *A&A*, 582, A33
 Barros, S. C. C., Almenara, J. M., Demangeon, O., et al. 2015, *MNRAS*, 454, 4267
 Bonavita, M., & Desidera, S. 2007, *A&A*, 468, 721
 Borucki, W. J., Koch, D., Basri, G., et al. 2010, *Science*, 327, 977
 Boyajian, T. S., LaCourse, D. M., Rappaport, S. A., et al. 2015, *ArXiv e-prints*, arXiv:1509.03622
 Brown, D. J. A., Anderson, D. R., Armstrong, D. J., et al. 2014, *ArXiv e-prints*, arXiv:1412.7761
 Burnham, S. W. 1882, *Publications of the Washburn Observatory*, 1, 92
 Carter, J. A., & Winn, J. N. 2009, *ApJ*, 704, 51
 Ciardi, D. R., Beichman, C. A., Horch, E. P., & Howell, S. B. 2015, *ApJ*, 805, 16
 Coughlin, J. L., Mullally, F., Thompson, S. E., et al. 2015, *ArXiv e-prints*, arXiv:1512.06149
 Daemgen, S., Hormuth, F., Brandner, W., et al. 2009, *A&A*, 498, 567
 Dekany, R., Roberts, J., Burruss, R., et al. 2013, *ApJ*, 776, 130
 Desidera, S., & Barbieri, M. 2007, *A&A*, 462, 345
 Dieterich, S. B., Henry, T. J., Golimowski, D. A., Krist, J. E., & Tanner, A. M. 2012, *AJ*, 144, 64
 Dressing, C. D., Adams, E. R., Dupree, A. K., Kulesa, C., & McCarthy, D. 2014, *AJ*, 148, 78
 Duchêne, G., & Kraus, A. 2013, *ARA&A*, 51, 269
 Eastman, J., Gaudi, B. S., & Agol, E. 2013, *PASP*, 125, 83
 Fischer, D. A., & Marcy, G. W. 1992, *ApJ*, 396, 178
 Fischer, D. A., Schwamb, M. E., Schawinski, K., et al. 2012, *MNRAS*, 419, 2900
 Foreman-Mackey, D., Montet, B. T., Hogg, D. W., et al. 2015, *ApJ*, 806, 215
 Garmany, C. D., Conti, P. S., & Massey, P. 1980, *ApJ*, 242, 1063
 Gazak, J. Z., Johnson, J. A., Tonry, J., et al. 2012, *Advances in Astronomy*, 2012, 30
 Gelman, A., & Rubin, D. B. 1992, *StaSc*, 7, 457
 Girardi, L., Groenewegen, M. A. T., Hatziminaoglou, E., & da Costa, L. 2005, *A&A*, 436, 895
 Hayward, T. L., Brandl, B., Pirger, B., et al. 2001, *PASP*, 113, 105
 Henden, A., & Munari, U. 2014, *Contributions of the Astronomical Observatory Skalnaté Pleso*, 43, 518
 Howell, S. B., Everett, M. E., Sherry, W., Horch, E., & Ciardi, D. R. 2011, *AJ*, 142, 19
 Howell, S. B., Sobeck, C., Haas, M., et al. 2014, *PASP*, 126, 398
 Kato, T., & Osaki, Y. 2014, *PASJ*, 66, L5
 LaCourse, D. M., Jek, K. J., Jacobs, T. L., et al. 2015, *MNRAS*, 452, 3561
 Lintott, C. J., Schawinski, K., Slosar, A., et al. 2008, *MNRAS*, 389, 1179
 Lintott, C. J., Schwamb, M. E., Barclay, T., et al. 2013, *AJ*, 145, 151

- Lodieu, N., Pérez-Garrido, A., Béjar, V. J. S., et al. 2014, *A&A*, 569, A120
- Mandel, K., & Agol, E. 2002, *ApJ*, 580, L171
- Mason, B. D., Wycoff, G. L., Hartkopf, W. I., Douglass, G. G., & Worley, C. E. 2001, *AJ*, 122, 3466
- Montet, B. T., Morton, T. D., Foreman-Mackey, D., et al. 2015, *ApJ*, 809, 25
- Mugrauer, M., & Neuhäuser, R. 2009, *A&A*, 494, 373
- Narita, N., Hirano, T., Fukui, A., et al. 2015, *ApJ*, 815, 47
- Ngo, H., Knutson, H. A., Hinkley, S., et al. 2015, *ApJ*, 800, 138
- Prša, A., Batalha, N., Slawson, R. W., et al. 2011, *AJ*, 141, 83
- Quintana, E. V., Adams, F. C., Lissauer, J. J., & Chambers, J. E. 2007, *ApJ*, 660, 807
- Raghavan, D., McAlister, H. A., Henry, T. J., et al. 2010, *ApJS*, 190, 1
- Roell, T., Neuhäuser, R., Seifahrt, A., & Mugrauer, M. 2012, *A&A*, 542, A92
- Sana, H., de Mink, S. E., de Koter, A., et al. 2012, *Science*, 337, 444
- Schlieder, J. E., Crossfield, I. J. M., Petigura, E. A., et al. 2016, *ArXiv e-prints*, arXiv:1601.02706
- Schmitt, J. R., Wang, J., Fischer, D. A., et al. 2014a, *AJ*, 148, 28
- Schmitt, J. R., Agol, E., Deck, K. M., et al. 2014b, *ApJ*, 795, 167
- Schwamb, M. E., Orosz, J. A., Carter, J. A., et al. 2013, *ApJ*, 768, 127
- Skrutskie, M. F., Cutri, R. M., Stiening, R., et al. 2006, *AJ*, 131, 1163
- Still, M., & Barclay, T. 2012, *PyKE: Reduction and analysis of Kepler Simple Aperture Photometry data*, *Astrophysics Source Code Library*, ascl:1208.004
- Tokovinin, A. 2014, *AJ*, 147, 87
- Tokovinin, A., & Cantarutti, R. 2008, *PASP*, 120, 170
- Tokovinin, A., Mason, B. D., & Hartkopf, W. I. 2010, *AJ*, 139, 743
- Tokovinin, A., Thomas, S., Sterzik, M., & Udry, S. 2006, *A&A*, 450, 681
- Torres, G., Fressin, F., Batalha, N. M., et al. 2011, *ApJ*, 727, 24
- Vanderburg, A., & Johnson, J. A. 2014, *PASP*, 126, 948
- Vanderburg, A., Latham, D. W., Buchhave, L. A., et al. 2015, *ArXiv e-prints*, arXiv:1511.07820
- Wang, J., Fischer, D. A., Xie, J.-W., & Ciardi, D. R. 2014, *ApJ*, 791, 111
- Wang, J., Fischer, D. A., Barclay, T., et al. 2013, *ApJ*, 776, 10
- . 2015, *ApJ*, 815, 127
- Wizinowich, P. L., Acton, D. S., Lai, O., et al. 2000, in *Society of Photo-Optical Instrumentation Engineers (SPIE) Conference Series*, Vol. 4007, Society of Photo-Optical Instrumentation Engineers (SPIE) Conference Series, ed. P. L. Wizinowich, 2–13
- Wright, E. L., Eisenhardt, P. R. M., Mainzer, A. K., et al. 2010, *AJ*, 140, 1868

APPENDIX

A. SELECTION BIASES

Table A1
Selections biases in target selection.

EPIC	Status	Detection ^a	General selection biases in order of GO proposals ^b
201160662	EBC		Late-FGK dwarfs
201207683	EBC		Red giants, but with overlap from KM dwarfs
201208431	VP		Red giants, but with overlap from KM dwarfs
201246763	EBC		Late-FGK dwarfs
201253025	EB		Late-FGK dwarfs — Known EBs
201257461	FP		Red giants, but with overlap from KM dwarfs
201270464	EBC		Metallic-line A stars — A0-F5 with a peculiar chemical composition, with pulsations, or in multiple star systems — A to early-F stars
201295312	PC		Late-FGK dwarfs
201324549	EBC	✓	Late-FGK dwarfs
201338508	VP		Late-FGK dwarfs — Red giants, but with overlap from KM dwarfs
201367065	VP		M-dwarfs — M-dwarfs — M-dwarfs (M0-M5) — M-dwarfs — Red giants, but with overlap from KM dwarfs — M-dwarfs — M-dwarfs (M0-M5)
201384232	VP		Late-FGK dwarfs
201393098	VP		Late-FGK dwarfs
201403446	PC		Late-FGK dwarfs
201407812	EBC		Late-FGK dwarfs
201408204	EB		Late-FGK dwarfs — Known EBs
201445392	PC		Red giants, but with overlap from KM dwarfs
201458798	EBC		Late-FGK dwarfs
201465501	VP		M-dwarfs — M-dwarfs — M-dwarfs, emphasizing M4 and later — Red giants, but with overlap from KM dwarfs — M-dwarfs, with the lower priority targets containing some likely M5-M8 dwarfs
201488365	EB		Known EBs (eclipsing Algols, EBs of the beta Lyr type, and EBs of the W Uma type) — Known EBs — Late-FGK dwarfs — Known EBs — F-dwarfs
201505350	CP		Late-FGK dwarfs
201516974	PHOI		Late-FGK dwarfs — Red giants, but with overlap from KM dwarfs
201546283	PC		Late-FGK dwarfs
201549860	PC		Red giants, but with overlap from KM dwarfs
201555883	FP		Red giants, but with overlap from KM dwarfs
201567796	EBC		Late-FGK dwarfs
201569483	FP		Late-FGK dwarfs — Red giants, but with overlap from KM dwarfs
201576812	EB		Late-FGK dwarfs — GKM dwarfs — Known EBs
201577035	VP		Late-FGK dwarfs
201594823	EB		Late-FGK dwarfs — Known EBs
201596316	VP		Late-FGK dwarfs — Red giants, but with overlap from KM dwarfs
201613023	VP		Late-FGK dwarfs
201617985	PC		M-dwarfs (M0-M6) with no 2MASS object within 10'' — Red giants, but with overlap from KM dwarfs
201626686	EBC		A to early-F stars — Late-FGK dwarfs
201629650	VP		Late-FGK dwarfs
201635569	VP		M-dwarfs, emphasizing M4 and later — Red giants, but with overlap from KM dwarfs
201648133	EBC		Late-FGK dwarfs
201649426	FP		Red giants, but with overlap from KM dwarfs
201665500	EB		Late-FGK dwarfs — Known EBs
201702477	PC		Red giants, but with overlap from KM dwarfs
201704541	EB	✓	Known EBs
201705526	EBC		Late-FGK dwarfs — F-dwarfs
201711881	EB		Cepheids — Late-FGK dwarfs
201725399	EBC		Known EBs
201736247	VP		Red giants, but with overlap from KM dwarfs
201754305	VP		Red giants, but with overlap from KM dwarfs
201779067	FP		Late-FGK dwarfs — GKM dwarfs
201826968	EBC	✓	Late-FGK dwarfs
201828749	PC	✓	Late-FGK dwarfs
201855371	VP		Red giants, but with overlap from KM dwarfs
201862715	CP	✓	Binaries from WDS with separation < 1.5'' — Solar-like planet-hosting stars — WASP-85 (late-FGK dwarfs) ^c — Late-FGK dwarfs — Red giants, but with overlap from KM dwarfs
201890494	EBC	✓	Late-FGK dwarfs
201912552	VP		M-dwarfs — M-dwarfs — M-dwarfs (M0-M5) — M-dwarfs (M0-M4) — M-dwarfs — M-dwarfs — Red giants, but with overlap from KM dwarfs — M-dwarfs (M0-M5)
201920032	PHOI		A0-F5 with a peculiar chemical composition, with pulsations, or in multiple star systems — Late-FGK dwarfs — F-dwarfs
201928968	EBC		Proper motion selected wide binaries > 5'' and < 120''
201929294	FP		Red giants, but with overlap from KM dwarfs
203533312	EB		Red giants, but with overlap from KM dwarfs — Late-FGK dwarfs — FGK dwarfs
204129699	EBC		Late-FGK dwarfs — FGK dwarfs
205924614	PHOI		Red giants, but with overlap from KM dwarfs
205985357	EBC		Red giants, but with overlap from KM dwarfs
206029314	EBC		Late-FGK dwarfs
206038483	PHOI		FGK dwarfs — Late-FGK dwarfs — A0-F5 stars that might be stars with a peculiar chemical composition, pulsating stars, or multiple star systems
206047297	PHOI		Red giants, but with overlap from KM dwarfs
206061524	PHOI	✓	Late-FGK dwarfs — Red giants, but with overlap from KM dwarfs — M-dwarfs

Table A1 — Continued

EPIC	Status	Detection ^a	General selection biases in order of GO proposals ^b
206082454	PHOI		FGK dwarfs — Late-FGK dwarfs
206135075	PHOI		FGK dwarfs — Late-FGK dwarfs — A0-F5 stars that might be stars with a peculiar chemical composition, pulsating stars, or multiple star systems
206135267	EB	✓	FGK dwarfs — Late M-dwarf EBs — GKM dwarfs — Late-FGK dwarfs — Red giants, but with overlap from KM dwarfs — A0-F5 stars that might be stars with a peculiar chemical composition, pulsating stars, or multiple star systems
206152015	PHOI	✓	Late-FGK dwarfs
206155547	PHOI		GKM dwarfs
206173295	PHOI		Late-FGK dwarfs
206245553	PHOI		FGK dwarfs — Late-FGK dwarfs
206247743	PHOI		Red giants, but with overlap from KM dwarfs
206311743	EBC		FGK dwarfs — Late-FGK dwarfs — Red giants, but with overlap from KM dwarfs
206380678	PHOI		Late-FGK dwarfs — Red giants, but with overlap from KM dwarfs
206432863	PHOI		Late-FGK dwarfs

Note. — CP is defined as confirmed planet, VP as validated planet, PC as planet candidate, PHOI as Planet Hunters Object of Interest, FP as fall positive, EB as a previously known eclipsing binary, and EBC as an EB candidate. All VPs, PCs, and FPs, and one CP (EPIC 201505350) are from Montet et al. (2015), while all other stars are from Planet Hunters.

^a Detected in this paper.

^b Selection biases between different GO proposals for the same star are separated by “—” in the same order as listed on the K2 website (Campaign 1: <http://keplerscience.arc.nasa.gov/K2/GuestInvestigationsC01.shtml> and Campaign 2: <http://keplerscience.arc.nasa.gov/K2/GuestInvestigationsC02.shtml>).

^c EPIC 201862715 was originally selected for by the WASP team based on its classification as a late-FGK dwarf. Its binarity was not taken into account for its selection (D. Brown 2015, private communication).